Mode-Division Multiplexing Over 96 km of Few-Mode Fiber Using Coherent 6×6 MIMO Processing

Roland Ryf, *Member, IEEE*, Sebastian Randel, *Senior Member, IEEE*, Alan H. Gnauck, *Fellow, IEEE, Fellow, OSA*, Cristian Bolle, Alberto Sierra, *Student Member, IEEE*, Sami Mumtaz, Mina Esmaeelpour, Ellsworth C. Burrows, René-Jean Essiambre, *Senior Member, IEEE, Fellow, OSA*, Peter J. Winzer, *Fellow, IEEE, Member, OSA*, David W. Peckham, *Senior Member, IEEE*, Alan H. McCurdy, *Member, IEEE*, and Robert Lingle, Jr., *Member, IEEE*

(Invited Tutorial)

***Abstract*—We report simultaneous transmission of six spatial and polarization modes, each carrying 40 Gb/s quadrature-phase-shift-keyed channels over 96 km of a low-differential group delay few-mode fiber. The channels are successfully recovered by offline DSP based on coherent detection and multiple-input multiple-output processing. A penalty of <1.2 dB is achieved by using 6×6 feed-forward equalizers with 120 taps each. The 6×6 impulse-response matrix fully characterizing the few-mode fiber is presented, revealing the coupling characteristics between the modes. The results are obtained using mode multiplexers based on phase plates with a mode selectivity of >28 dB.**

***Index Terms*—Digital signal processing (DSP), MIMO, optical fibers.**

I. INTRODUCTION

AFTER growing for over two decades by about three orders of magnitude, the capacity of single-mode fibers (SMFs) is rapidly approaching the capacity limits imposed by the combination of Shannon's information theory and nonlinear fiber effects [1]. The success of this capacity growth can be largely attributed to wavelength division multiplexing, polarization-division multiplexing (PDM), and higher order modulation formats [2]. In order to keep up with the demands in traffic growth, a new dimension is now required and it has recently been suggested [3] that space-division multiplexing (SDM) be used as a technique to sustain the capacity growth in optical transmission systems. In SDM, spatially separated channels are used to transmit multiple signals, and SDM over a single fiber is of particular interest because of the potential cost, space, and energy savings [4]. SDM over a single fiber can be realized by exploiting multiple fiber-waveguide modes, and earlier attempts [5], [6] were limited in transmission distance and bandwidth by the lack of highly selective mode couplers that allow selective excitation of all waveguide modes, as well as the impact of modal differential group delay (DGD). In more recent experiments, mode-division multiplexing was successfully applied to increase distance and capacity by using mode multiplexing in few-mode fibers (FMFs)[7]–[9]. However, these reports only make use of a subset of the fiber-waveguide modes. Maximum single-fiber SDM capacity gains, realized by making use of the full set of fiber-waveguide modes, has been demonstrated for the first time using two different approaches. The first approach is based on multicore fibers, where the crosstalk between cores has been almost completely suppressed by fiber design, thus allowing to treat the individual cores as independent waveguides [10], [11]. The second approach is based on multiple-input multiple-output (MIMO) signal processing in combination with coherent detection. In contrast to earlier MIMO experiments conducted over multimode fiber (MMF)[7], [8], [12], the complete set of waveguide modes supported by the MMF is launched and coherently detected. This offers the major advantage of realizing maximum single-fiber SDM capacity gain and high reliability (i.e., low outage) at the same time [13], [14].

In this paper, we present SDM transmission over an FMF supporting six spatial- and polarization modes, referred in the following as six-mode FMF. In order to clarify our nomenclature of the modes, Fig. 1 lists the six fiber-waveguide modes of the six-mode FMF according to [15] and [16] on the first column, and its relation to the linearly polarized (LP) mode LP_{01} and the twofold degenerate LP_{11} mode listed in the forth column.

Manuscript received September 02, 2011; accepted October 13, 2011. Date of publication November 09, 2011; date of current version February 01, 2012.

R. Ryf, S. Randel, A. H. Gnauck, A. Sierra, E. C. Burrows, R.-J. Essiambre, and P. J. Winzer are with Bell Laboratories, Alcatel-Lucent, Holmdel, NJ 07733 USA (e-mail: roland.ryf@alcatel-lucent.com; sebastian.randel@alcatel-lucent.com; alan.gnauck@alcatel-lucent.com; sierranoguera@gmail.com; ells.burrows@alcatel-lucent.com; rene.essiambre@alcatel-lucent.com; peter.winzer@alcatel-lucent.com).

C. Bolle is with the Microsystems and Nanotechnology Research Department, Bell Laboratories, Alcatel-Lucent, Murray Hill, NJ 07974 USA (e-mail: Cristian.Bolle@alcatel-lucent.com).

S. Mumtaz is with the Institute of Optics, University of Rochester, Rochester, NY 14627 USA (e-mail: sami.mumtaz@optics.rochester.edu).

M. Esmaeelpour is with the Department of Physics, Lehigh University, Bethlehem, PA 18015 USA (e-mail: mie210@lehigh.edu).

D. W. Peckham and A. McCurdy are with OFS, Norcross, GA 30071 USA (e-mail: dpeckham@ofsoptics.com; mccurdy@ofsoptics.com).

R. Lingle, Jr., is with OFS, Norcross, GA 30071 USA, and also with the Department of Electrical and Computer Engineering, Georgia Institute of Technology, Altanta, GA 30332 USA (e-mail: rlingle@ofsoptics.com).

Color versions of one or more of the figures in this paper are available online at http://ieeexplore.ieee.org.

Digital Object Identifier 10.1109/JLT.2011.2174336

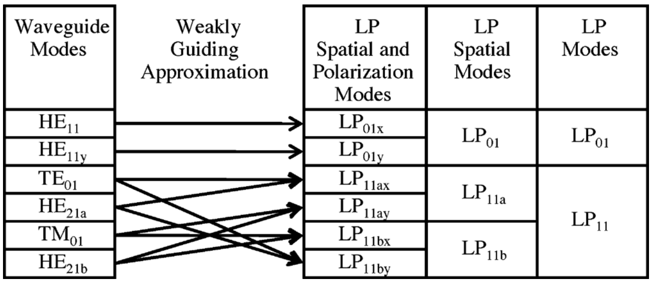

Fig. 1. Relation between the LP modes and the real waveguide modes $\mathrm{HE}_{11\mathrm{x}}$, $\mathrm{HE}_{11\mathrm{y}}$, TE_{01}, TM_{01}, $\mathrm{HE}_{21\mathrm{a}}$, and $\mathrm{HE}_{21\mathrm{b}}$ of the six-mode FMF.

$\mathrm{LP}_{11\mathrm{a}}$ and $\mathrm{LP}_{11\mathrm{b}}$ are used to distinguish the degenerate LP_{11} mode, and the suffix "x" and "y" in the indexes are used to distinguish the two orthogonal linear polarizations.[1] The six-mode FMF allows for six independent data channels to be simultaneously transmitted at a single wavelength. The six data channels are launched polarization multiplexed into the LP_{01}, the $\mathrm{LP}_{11\mathrm{a}}$, and the $\mathrm{LP}_{11\mathrm{b}}$ spatial mode, using a mode multiplexer with high mode selectivity (>28 dB). The mode multiplexer is based on phase masks [17], [18] fabricated in glass, which is a simple yet effective alternative to multiplexers based on programmable spatial light modulators [8], [19]. Our design offers low crosstalk and low polarization dependence. After transmission, a second mode multiplexer is used to separate the received optical field into three spatial channels that are detected by three synchronized coherent receivers with polarization diversity. In order to recover the transmitted data, 6×6 MIMO DSP [20], [21] is applied to undo coupling effects occurring within the fiber. MIMO processing compensates linear impairments like dispersion, crosstalk, and DGD between modes and polarizations.

In this paper, we report a major advancement in single-fiber SDM transmission by increasing the transmission length from previously reported 10 km in [22] and 33 km in [21] to a length of 96 km, at a penalty of <1.2 dB. In Sections II and III, we describe the characteristics of the low-DGD six-mode FMF and the mode multiplexer based on phase plates, respectively. In Section IV, we describe the experimental setup for the SDM transmission measurement. Further, in Section V, we present an impulse-response matrix measurement for the three-mode fiber, which completely characterizes the instantaneous linear mode coupling, and finally Section VI describes the offline MIMO DSP algorithms and resulting bit error rate (BER) estimates.

II. LOW-DGD THREE-MODE FIBER

In order for the MIMO DSP described in Section VI to be implementable, the time delay between the received SDM channels has to be kept sufficiently small, because any time delay has to be compensated by an equalizing filter with a finite number of taps. Therefore, an essential requirement for the six-mode FMF is to reduce the DGD as much as possible. The low-DGD six-mode FMF used in this paper is based on a depressed cladding index profile with normalized frequency $V \approx 5$, following the conventional definition $V = \pi d/\lambda \sqrt{n_1^2 - n_2^2}$, with the core diameter d, the wavelength of light in free space λ, and the refractive indexes n_1 and n_2 of core and cladding, respectively. The design is optimized to stabilize the LP_{11} mode, to effectively cutoff the LP_{21} and LP_{02} modes, and to minimize the DGD across the *C*-band. The resulting fiber has a loss coefficient, measured by optical time-domain reflectometry of 0.205 dB/km at 1550 nm; no significant mode-dependent loss is observed. The effective areas of the LP_{01} and LP_{11} modes are calculated to be approximately 155 and 159 $\mu\mathrm{m}^2$, respectively. The chromatic dispersion is calculated based on the fiber parameters to be around 18 ps/(nm km) for both LP_{01} and LP_{11} modes.

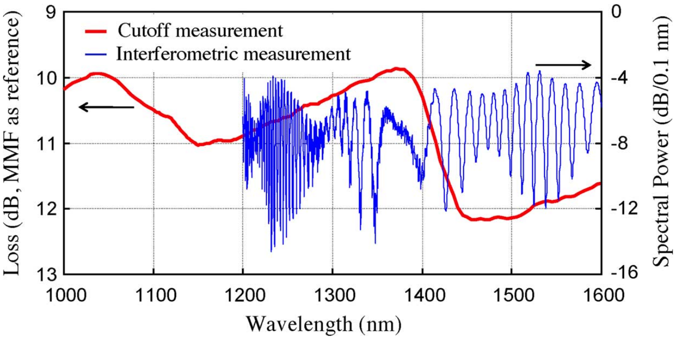

Fig. 2. Mode excitation measurements performed on a 10 m FMF to determine the number of propagating modes. See the text for explanation.

The number of modes guided by the FMF is determined by measuring the spectral transmission loss through a short length of fiber and correlating the results with an interferometric measurement. The transmission loss measurement is made using an overfilled launch condition and referenced to a 2 m MMF sample. The loss, relative to the 2 m reference, is shown as the thick curve in Fig. 2 for a 10 m long FMF. Cutoff wavelengths of various modes are found from the positions of the edges of the stair steps (found at $\sim$1100 and $\sim$1400 nm). No steps in transmitted power are observed above 1400 nm, up to 1700 nm, which is the limit of the test apparatus. From the normalized frequency V of this fiber, however, it is deduced that both LP_{01} and LP_{11} modes are present at 1550 nm (the LP_{11} cutoff is predicted to be around 1800 nm). This is confirmed by the interferometric measurement, shown as the thin curve in Fig. 2, where an SMF is offset spliced to each end of a 10 m FMF. The incoming light excites both the fundamental and higher order modes in the FMF which, due to different group velocities, interfere at the splice between the FMF and the downstream SMF. The intensity pattern produced by the interference is wavelength dependent and produces a nearly sinusoidal pattern for each corresponding interfering modal pair. Above 1400 nm, the thin curve plotted in Fig. 2 shows a single periodic function with slowly changing amplitude envelope, indicating that only two modes are present in the fiber. Below 1400 nm, the fast changes in intensity of the interferometric measurements plotted in Fig. 2 confirm the presence of a new propagating mode. The additional mode will create a superposition of three sinusoidal intensity patterns with periods related to the DGD of the three possible modal pairs.

---

[1] $\mathrm{HE}_{11\mathrm{x}}$, $\mathrm{HE}_{11\mathrm{y}}$, TE_{01}, TM_{01}, $\mathrm{HE}_{21\mathrm{a}}$, and $\mathrm{HE}_{21\mathrm{b}}$, are the real waveguide modes of the six-mode FMF; however, our mode multiplexer excites LP modes, which can be represented in good approximation as a linear combination of the real waveguide modes.

Note that the interference between LP_{01} and LP_{11} still dominates in this region. Note also that the period of the sinusoidal modulation is wavelength dependent, and the periods for interference between the LP_{01} and LP_{11} modes become very long near 1370 nm. The DGD between the lowest order modes is found using the interferometric setup just described. The relationship between the DGD and the measured wavelength period $\Delta\lambda$ of the transmitted power spectral density can be derived considering the wavelength dependence of the relative phase shift $\Delta\Phi$ between the LP_{01} and LP_{11} modes [23] after a length L of the FMF; this phase shift is given by

$$\Delta\Phi = 2\pi\Delta n_{\mathrm{eff}} L/\lambda \tag{1}$$

where Δn_{eff} is the difference in effective index between the LP_{01} and LP_{11} modes. Two wavelengths, λ_0 and λ, respectively, will result in the same interference if

$$\Delta\Phi(\lambda) - \Delta\Phi(\lambda_0) = 2\pi k \tag{2}$$

where k is an integer. Note that the index difference Δn_{eff} in (1) in general also shows a small wavelength dependence due to material- and waveguide dispersion effects. This wavelength dependence is approximated by the following Taylor expansion of Δn_{eff} at the wavelength λ_0:

$$\Delta n_{\mathrm{eff}}(\lambda) \approx \Delta n_{\mathrm{eff}}(\lambda_0) + (\lambda - \lambda_0)\left.\frac{\partial \Delta n_{\mathrm{eff}}}{\partial \lambda}\right|_{\lambda_0}. \tag{3}$$

Using (1) and (3) in (2) and setting $k = 1$, gives the following relation for the wavelength period $\Delta\lambda$ of the interference spectrum:

$$\Delta\lambda = \lambda - \lambda_0 = -\lambda_0^2/(\Delta n_{\mathrm{g}}(\lambda_0)L + \lambda_0). \tag{4}$$

Here, the group index difference Δn_{g} has been introduced, which is conventionally defined as

$$\Delta n_{\mathrm{g}}(\lambda_0) = \Delta n_{\mathrm{eff}}(\lambda_0) - \lambda_0\left.\frac{\partial \Delta n_{\mathrm{eff}}}{\partial \lambda}\right|_{\lambda_0}. \tag{5}$$

Introducing the length-specific DGD: $\mathrm{DGD}_{\mathrm{L}} = \mathrm{DGD/L}$, which is related to the group index difference by $\mathrm{DGD}_{\mathrm{L}} = \Delta n_{\mathrm{g}} c$, we find

$$|\mathrm{DGD}_{\mathrm{L}}| = \frac{\lambda_0^2}{|\Delta\lambda| Lc} \tag{6}$$

where $\lambda_0/\Delta\lambda \gg 1$ has been used, and only the magnitude of the DGD is actually measured.

Fig. 3 shows the absolute magnitude of the derived $\mathrm{DGD}_{\mathrm{L}}$ for various lengths of the FMF as a function of wavelength. The longest fiber (980 m) creates the longest interferometer which results in a spectrum with very rapid oscillations. This is useful for determining the DGD near 1370 nm, where the LP_{01} and LP_{11} have zero DGD and, therefore, have essentially the same transit time through the FMF.

The DGD between the LP_{01} mode and the LP_{11} mode was also measured by launching a 100 ps intensity-modulated probe pulse simultaneously into the LP_{01} and the $\mathrm{LP}_{11\mathrm{a}}$ spatial mode, and by simultaneously detecting the LP_{01} and the $\mathrm{LP}_{11\mathrm{a}}$ mode after 96 km of fiber. This is experimentally realized by intentionally misaligning the phase plate position in the mode multiplexer presented in Section III. The probe pulse corresponding to the LP_{01} mode is observed to arrive first and the DGD is within 2.6 ± 0.1 ns over the wavelength range of 1530 to 1565 nm, corresponding to a $\mathrm{DGD}_{\mathrm{L}} = 27$ ps/km. This value is approximately two times smaller than the $\mathrm{DGD}_{\mathrm{L}}$ measured in the short fiber. A possible explanation for the discrepancy is that the $\mathrm{DGD}_{\mathrm{L}}$ may vary along the fiber due to variation in the fiber parameters. Alternatively, the coupling between LP_{01} and the LP_{11} modes could also cause a reduction of the observed DGD at longer distances, in analogy to the distance dependence of the polarization mode dispersion as observed in SMFs.

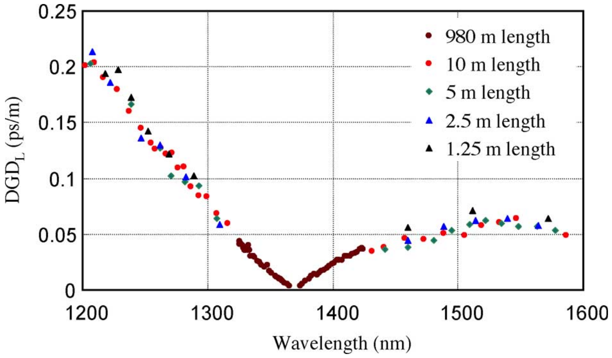

Fig. 3. DGD measurements performed on short FMFs plotted for different length. See the text for explanation.

Distributed microbend coupling between guided modes or between guided and leaky modes during propagation leads to crosstalk between guided modes and power loss from guided modes, respectively. The dependence of the coupling strength between modes can be approximated by various powers of the modal propagation constant difference $\Delta\beta^{-p}$ with $p \geq 4$ [24]. The resulting coupling within the degenerate LP_{11} mode will be much stronger than between LP_{11} and LP_{01}.

III. MODE MULTIPLEXER BASED ON PHASE PLATES

In order to achieve the maximal SDM capacity gain, the complete set of modes supported by the six-mode FMF fiber has to be excited without significant crosstalk [13]. We hence built spatial-mode multiplexers (MMUXs) to couple the light from multiple SMFs into the different spatial modes of the six-mode FMF. A practical way to selectively couple light into a LP_{11} mode was shown in [17] and [18]. A phase plate whose phase profile matches the phase of the target mode is inserted into the optical path between the incoming beam and the six-mode FMF. The theoretical intensity and phase profiles of the LP spatial modes of a six-mode FMF are shown in Fig. 4(c) and (d), respectively. The LP_{01} mode (first column in Fig. 4) has a flat phase front and can, therefore, be directly coupled into the six-mode FMF from the output of an SMF. Coupling into the LP_{11} mode will require a phase plate that introduces a phase jump of π between two half planes. Two orthogonal orientations are possible, as indicated in columns 2 and 3 in Fig. 4, designated as $\mathrm{LP}_{11\mathrm{a}}$

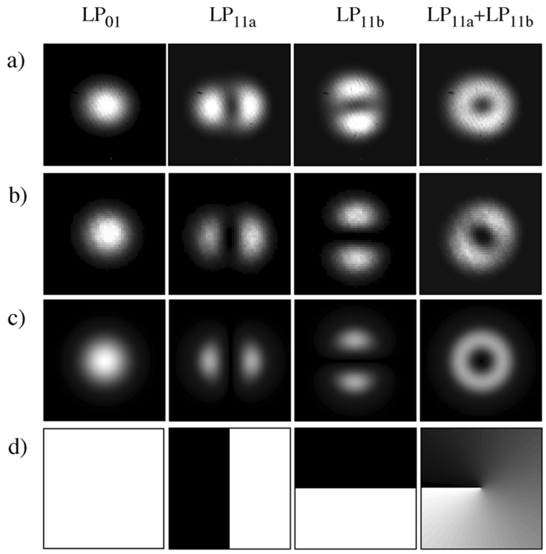

Fig. 4. Measured mode intensity profile after (a) 96 km and (b) 33 km six-mode FMF for different launched input modes and fiber configurations (see the text for a detailed description). (c) Theoretical mode intensity profiles for a six-mode FMF and (d) corresponding phase profiles.

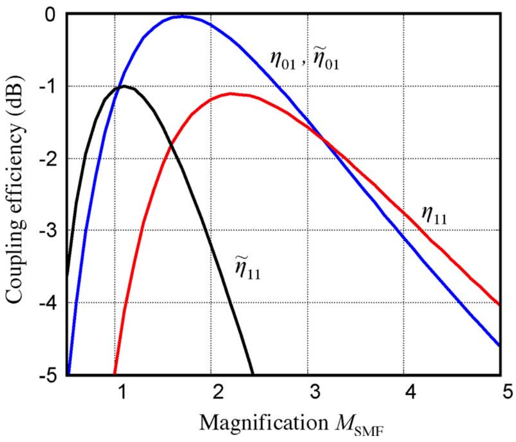

Fig. 5. Theoretical coupling efficiency for phase-plate-based coupler. See the text for explanation.

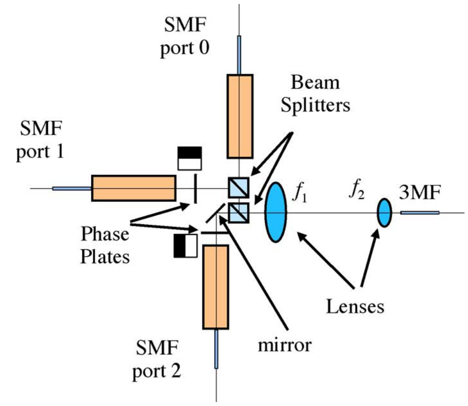

Fig. 6. Schematic setup of the six-mode FMF mode multiplexer.

and LP_{11b}, respectively. Generally, the phase plate can be inserted at two different locations along the optical path, corresponding either to the image plane or the Fourier plane of the end facet of the six-mode FMF. The spatial Fourier transforms of the linear polarized fiber mode amplitude profiles have the interesting property of being similar to their originating amplitude profile [25]. In particular, the phase structure is maintained and also the intensity profile is similar. Therefore, the same phase plates can be placed either in the Fourier plane or image plane to achieve mode conversion, and the most convenient optical arrangement can be selected. In contrast to [17] and [18], which have the phase plates in the Fourier plane, the phase plates are located in the image plane for our couplers. The coupling efficiency η_{nm} for coupling from an SMF into the LP_{nm} mode of an MMF for phase plates located in the image plane can be calculated using the overlap integral [26]

$$\eta_{nm} = \left| \iint\limits_{-\infty}^{+\infty} \chi_{\mathrm{SMF}}(x,y)\phi_{nm}(x,y))\psi^*_{nm}(x,y)dxdy \right|^2 \tag{7}$$

where χ_{SMF} is the normalized complex amplitude proportional to the electrical field generated by the SMF on the facet of the six-mode FMF after traversing the optical system, normalized to $\iint\limits_{-\infty}^{+\infty} |\chi_{\mathrm{SMF}}(x,y)|^2 dxdy = 1$. For most practical applications, χ_{SMF} can be approximated by a Gaussian beam. The phase plate transfer function ϕ_{nm} has an amplitude $|\phi_{nm}(x,y)| = 1$ and will be typically set to $\phi_{nm}(x,y) = \psi_{nm}(x,y)/|\psi_{nm}(x,y)|$, where ψ_{nm} is the normalized complex amplitude of the electrical field of the corresponding LP_{nm} mode, and * denotes complex conjugation. The coupling efficiency $\tilde{\eta}_{nm}$ for the case when the phase plate is located in the Fourier plane can be calculated by replacing χ_{SMF} and ψ_{nm} with their Fourier transform complex amplitudes $\tilde{\chi}_{\mathrm{SMF}}$ and $\tilde{\psi}_{nm}$, respectively. The coupling efficiencies for both arrangements are shown in Fig. 5 for the case when a standard SMF is coupled into a six-mode FMF with step index profile with core diameter of 16 μm and normalized frequency $V = 5$. The coupling efficiencies are plotted as a function of the magnification M_{SMF} defined as the magnification between SMF and step index six-mode FMF. The coupling efficiency for coupling into the LP_{01} mode is the same for the phase plates located in the Fourier plane or image plane and shows a maximum coupling very close to 0 dB for a magnification of 1.7. When coupling into the LP_{11} mode, the maximum coupling efficiencies are -1 and -1.1 dB for the phase plates located in the Fourier plane and image plane, respectively. Even if the arrangement with phase plates located in the Fourier plane has a slightly lower loss, the image plane arrangement offers the practical advantage of being more tolerant toward errors in the magnification factor.

In order to excite multiple modes simultaneously, beam splitters are used. The experimental arrangement of the MMUX is shown in Fig. 6. The MMUX has three ports consisting of three collimators with a nominal full-width at half-maximum (FWHM) beam diameter of 500 μm, where the light from port 0 is directly coupled into the LP_{01} mode of the six-mode FMF, and ports 1 and 2 have orthogonal phase plates inserted in their optical path and will, hence, launch into the LP_{11a} and LP_{11b} spatial modes, respectively. The phase plates are imaged on the facet of the six-mode FMF using a double telecentric optical imaging system, formed by a lens pair with focal length $f_1 = 75$ mm and $f_2 = 3.9$ mm, respectively.

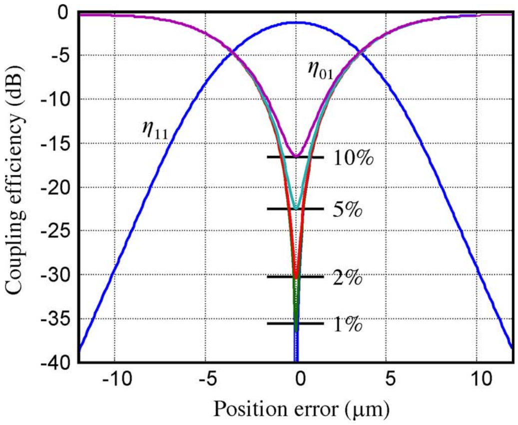

Fig. 7. Theoretical coupling efficiencies η_{11} and η_{01} for misaligned phase plates, plotted for different phase-plate thickness-difference errors of 0%, 1%, 2%, 5%, and 10%.

The phase plates are fabricated of 0.7 mm thick Borosilicate glass, and a photolithographic process is used to create the phase pattern, which in a following step is etched into the glass in order to achieve the desired thickness difference d. The resulting phase difference is given by

$$\Delta\varphi = \frac{2\pi d}{\lambda}(n_{\mathrm{gl}} - 1) \tag{8}$$

where λ is the wavelength of light and $n_{\mathrm{gl}} = 1.455$ is the refractive index of the Borosilicate glass. Setting the phase difference $\Delta\varphi = \pi$, and solving (8) with respect to d we obtain

$$d = \frac{\lambda}{2(n_{\mathrm{gl}} - 1)} = 1.703\ \mu\mathrm{m}. \tag{9}$$

The thickness difference of the plates was verified using an optical profilometer and found to be within 1% of the required thickness difference.

The impact of the thickness-difference error and lateral alignment error of the phase plate is shown in Fig. 7, where the coupling efficiencies η_{11} and η_{01} are shown as a function of the position error and different thickness-difference errors. An error of thickness difference of 1% will produce a crosstalk < -35 dB; however, the lateral error is more critical and submicron precision is required to achieve good mode selectivity.

The three beams are combined using two beam splitters with a reflectivity of 50% and a transmittance of 38%. We define the MMUX coupling loss as the power exiting a short (2 m) 6-mode FMF compared to the power launched into the SMF of the corresponding MMUX port. Coupling losses of 9.6, 9, and 7.8 dB are measured for the LP_{01}, $\mathrm{LP}_{11\mathrm{a}}$, and $\mathrm{LP}_{11\mathrm{b}}$ spatial modes, respectively. The loss variation between the modes is produced by the ratio and loss of the beam splitter and the mode coupling efficiencies η_{01} and η_{11}. The latter can be optimized by changing the magnification M_{SMF} as shown in Fig. 5. In our arrangement the magnification is given by

$$M_{\mathrm{SMF}} = \frac{D_{\mathrm{Col}}}{D_{\mathrm{SMF}}}\frac{f_2}{f_1} \tag{10}$$

where D_{SMF} and D_{Col} are the FWHM diameter of the light intensity profile at the exit of the SMF and the collimator, respectively. In general, the loss L_n for the three ports can be written as

$$L_0 = \eta_{01}(1 - \kappa_1)\kappa_2 \tag{11}$$

$$L_1 = \eta_{11}(1 - \kappa_1)(1 - \kappa_2) \tag{12}$$

$$L_2 = \eta_{11}\kappa_1 \tag{13}$$

where κ_1 and κ_2 are the splitting ratio of the first and second beam splitter, respectively. Here, we assume a lossless beam splitter and $\kappa_n = 1$ is equivalent to 100% transmission. The loss of all three ports is minimal when the condition $L_0 = L_1 = L_2$ is fulfilled. In that case, (13) can be solved with respect to κ_1 and κ_2 and we obtain

$$\kappa_{1,\min} = \frac{\eta_{01}}{2\eta_{01} + \eta_{11}} \tag{14}$$

and

$$\kappa_{2,\min} = \frac{\eta_{11}}{\eta_{01} + \eta_{11}} \tag{15}$$

and the resulting minimal loss is given by

$$L_{\min} = \frac{\eta_{01}\eta_{11}}{2\eta_{01} + \eta_{11}}. \tag{16}$$

Assuming that the magnification M_{SMF} for the LP_{01} and the LP_{11} spatial modes is independently optimized, for example, by using collimators with different beam diameters for the respective ports, we obtain a 5.5 dB minimum theoretical loss for the coupler arrangement.

Next, we measure modal crosstalk of the MMUX. Since the power coupled into each mode of a six-mode FMF can most conveniently be determined using another MMUX at the fiber output, we consider the crosstalk of an MMUX *pair* as opposed to that of a single MMUX. We hence define the crosstalk of an MMUX pair as the ratio of the power measured at the launch-mode port of the output MMUX to the largest power measured in any of the other ports of the output MMUX. Input and output MMUXs are connected by a short (2 m) six-mode FMF such that mode coupling inside the fiber can be neglected. We measure a crosstalk suppression from the LP_{01} spatial mode to the LP_{11} spatial mode of >28 dB. Fig. 4(a) and (b) presents pictures of the modes measured by imaging the end facet of the six-mode FMF using an InGaAs infrared camera after 33 and 96 km of fiber, respectively. Simulated mode intensity images are reported in Fig. 4(b) and show good qualitative agreement between theory and experiment for 33 km of six-mode FMF. Note that when launching power into one of the two LP_{11} modes, the output mode distribution will typically be a linear combination of all LP_{11} spatial and polarization modes, which are continuously mixed along propagation in the fiber as a result of being linear combinations of the real waveguide fiber modes (see Fig. 1). By moving, bending, or changing the temperature of the six-mode FMF, the relative phase between the LP_{11} spatial and polarization modes can be changed. In order to capture the images shown in Fig. 4, the six-mode FMF was twisted and bent using 10 cm diameter loops until the desired image resembling a pure mode was obtained. When launching the LP_{01}

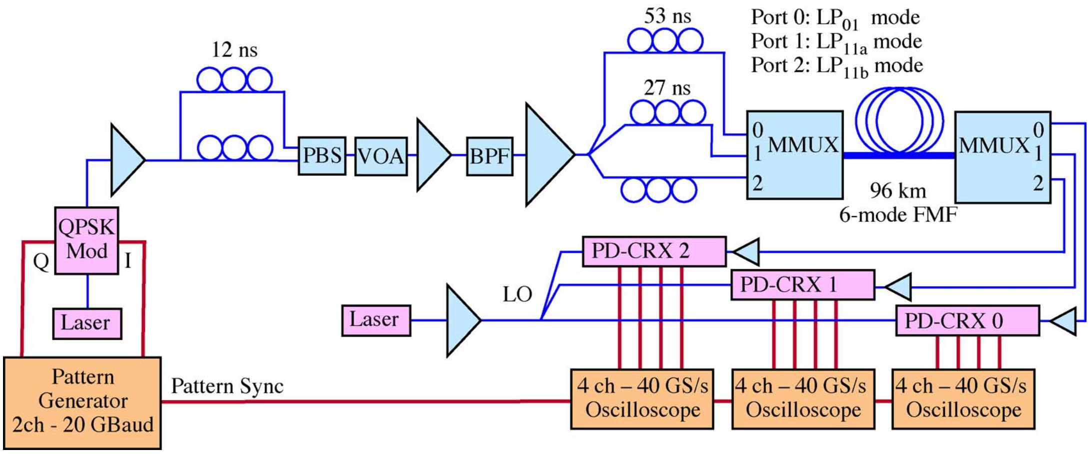

Fig. 8. Experimental setup. QPSK-Mod: QPSK modulator, PBS: polarization beam splitter, VOA: variable optical attenuator, BPF: bandpass filter, LO: local oscillator, and PD-CRX: polarization-diversity coherent receiver.

mode, twisting and bending the fiber has no noticeable effect, confirming the low coupling between LP_{01} and LP_{11} modes. This was further confirmed by repeating the crosstalk measurements with 33 and 96 km of six-mode FMF, which resulted in a typical “MMUX-plus-fiber” crosstalk fluctuating around -18 and -11 dB, respectively. After 33 km, the crosstalk is small enough as to not be noticeable in the mode images in Fig. 4(b), whereas for 96 km, it is clearly noticeable that the contrast of the mode profile is reduced. In particular, the center of the image, where the LP_{01} mode has its maximum, is not completely dark anymore. Even if the noticeable crosstalk in Fig. 4(a) is modest, the crosstalk produces a significant transmission penalty if left uncorrected, as shown in Section VI. Note that no particular mode alignment is performed in preparation of the transmission experiment, as the MIMO DSP is capable of separating the different degenerate modes, in analogy to the polarization separation obtained by the receiver in a coherent polarization-multiplexed system.

IV. EXPERIMENTAL SETUP FOR SDM TRANSMISSION

The transmission-measurement setup is shown in Fig. 8. As a test signal, we use a quadrature-phase-shift-keyed (QPSK) signal. The in-phase (I) and quadrature (Q) components of the QPSK signal are two independent De Bruijn bit sequences of length 2^{12}. This has the advantage of avoiding correlation effects as described in [21] and [27]. The signal is generated using a two-channel pattern generator operated at 20 Gbaud to drive a double-nested LiNbO_3 Mach–Zehnder modulator. As a light source, we use an external cavity laser (ECL) with 100 kHz linewidth operating at 1560 nm. A polarization-multiplexer stage with a delay of 12 ns creates a PDM-QPSK signal which is then connected to a noise-loading section consisting of a variable optical attenuator (VOA) in front of an erbium-doped fiber amplifier (EDFA), followed by an optical bandpass filter (BPF) with a bandwidth of 1.3 nm and an additional high-power EDFA. Three different copies of the PDM-QPSK signal with a relative delay of 27 and 53 ns are then generated and connected to different ports of the input MMUX. The six-mode FMF port of the MMUX is connected to 96 km of six-mode FMF and terminated by a second MMUX acting as a mode demultiplexer. The power launched into the six-mode FMF was 6 dBm from each port. The three SMF ports of the second MMUX are amplified by low-noise EDFAs before entering three polarization-diversity coherent receivers (PD-CRX). Each PD-CRX consists of a polarizing beam splitter to separate the received signal in two polarizations, followed by two optical hybrids whose output ports are connected to a total of four balanced receivers for each PD-CRX. Three PD-CRXs are required, resulting in 12 electrical high-speed signals that are captured using three high-speed digital oscilloscopes with four ports each, operating at a sampling rate of 40 GS/s. The oscilloscopes have a bandwidth of 15 GHz for PD-CRX 0 and 16 GHz for PD-CRX1 and PD-CRX2, respectively. For each measurement, a total of four million samples are captured and a common trigger signal produced by the pattern generator is used to start the simultaneous data acquisition on all three oscilloscopes. A second ECL is used as a local oscillator (LO) in an intradyne configuration. The LO frequency was adjusted to within ±20 MHz of the central frequency of the received signal.

The performance of the setup is verified first with a back-to-back (B2B) measurement, where the MMUXs are temporarily disconnected and the corresponding SMFs are bridged with three fiber jumpers. The measurement results for transmission are presented in Section VI. In the following section, we first present a complete characterization of the fiber impulse-response matrix at one point in time.

V. IMPULSE-RESPONSE MATRIX MEASUREMENT OF THE SIX-MODE FMF

The six-mode FMF can be described as a 6×6 MIMO channel, which in the linear case is fully characterized by its 6×6 impulse-response matrix $\mathbf{H}$. The elements of $\mathbf{H}$ consist of 36 impulse-responses $\mathbf{h}_{nm}$, where n is the index of the receive port and m is the index of the transmitted port. Each impulse response can be described as a vector $\mathbf{h}_{nm} = [h_{nm}(1) \dots h_{nm}(L)]$ with length L. Although it is not necessary to characterize the impulse-response matrix in

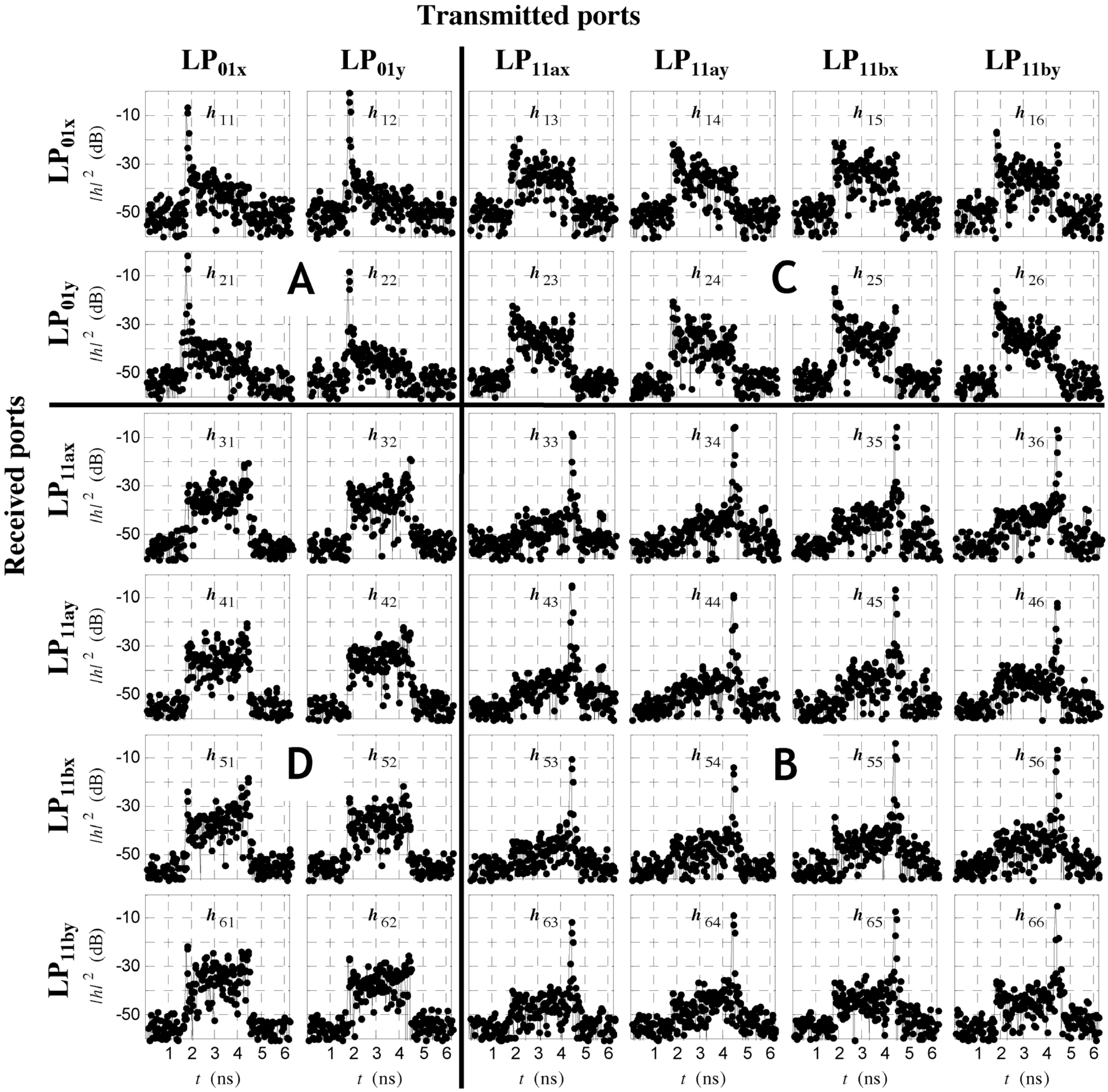

Fig. 9. Squared magnitude of the PDM-SDM 6 × 6 impulse responses for 96 km of six-mode FMF. See the text for explanation.

order to perform the MIMO equalization described in the next section, doing so gives a deeper insight into the strength of the mode coupling between LP spatial and polarization modes. Furthermore, this characterization helps to explain where within the link mode coupling actually happens. The impulse response $\mathbf{h}_{nm}$ can be determined using a test signal $s_m(k)$, where m denotes the transmit channel and k is the symbol (time) index. Furthermore, we define $r_n(k)$ as the nth received channel. The estimation of the impulse-response matrix is referred to as channel estimation in MIMO literature, and numerous algorithms are available [28]. The channel estimation results presented in Fig. 9 are based on the least square error (LSE) estimator. This choice is motivated by the better estimation accuracy observed if compared to the least mean square error (LMS) estimator described in [21]. In order to perform the channel estimation based on the LSE estimator, it is convenient to rearrange $\mathbf{h}_{nm}(k)$, $r_n(k)$, and $s_n(k)$ in the following way:

$$\mathbf{r}_n = [r_n(1) \ldots r_n(n_{\mathrm{tr}} - L + 1)]^{\mathrm{T}} \tag{17}$$

$$\mathbf{h}_n = [\mathbf{h}_{n1} \ldots \mathbf{h}_{nN}]^{\mathrm{T}} \tag{18}$$

$$\mathbf{S}_m = \begin{bmatrix} s_m(L) & \ldots & \ldots & s_m(1) \\ s_m(L{+}1) & s_m(L) & \ldots & s_m(2) \\ \vdots & \ddots & & \vdots \\ s_m(n_{\mathrm{tr}}) & \ldots & \ldots & s_m(n_{\mathrm{tr}} - L + 1) \end{bmatrix} \tag{19}$$

$$\mathbf{S} = [\mathbf{S}_1 \ldots \mathbf{S}_N] \tag{20}$$

where $\mathbf{r}_n$ is a column vector, the concatenation of impulse responses $\mathbf{h}_n$ is also a column vector, $N = 6$ is the number of input and output channels, n_{tr} is the size of the training sequence for each channel, $\mathbf{S}$ is an $(n_{\mathrm{tr}} - L + 1) \times (LN)$ matrix consisting of a concatenation of the matrices S_m, and $^{\mathrm{T}}$ means transposed. The received symbols can then be expressed as the matrix equation

$$\mathbf{r}_n = \mathbf{S_n} \quad \mathbf{h}_n + \boldsymbol{\nu} \tag{21}$$

where $\boldsymbol{\nu}$ describes noise added to the system. The estimate $\hat{\mathbf{h}}_n$ that minimizes $\|\hat{\mathbf{h}}_n - \mathbf{h}_n\|^2$ according to the LSE norm denoted by $\|\cdots\|^2$ is given by [28]

$$\hat{\mathbf{h}}_n = (\mathbf{S}^H \mathbf{S})^{-1} \mathbf{S}^H \mathbf{r}_n \tag{22}$$

where ^{H} denotes the conjugate transpose. (22) can be evaluated, and an estimate for the impulse-response matrix $\mathbf{H}$ can be determined. The squared magnitude of the 6×6 impulse responses are shown in Fig. 9. In this representation, the columns correspond to the transmitted ports, and the rows to the received ports, respectively. In order to show the impulse responses only due to mode coupling, the chromatic dispersion of 96×18 ps/nm was electronically compensated on the received signal $r_i(k)$ prior to estimating the impulse-response matrix. This results in sharp peaks that clearly identify the main coupling points. Fig. 9 can be divided into four regions designated with A, B, C, and D: Region A is the 2×2 array located at the top left corner and is formed by the impulse-response matrix elements (h_{11}, h_{12}, h_{21}, h_{21}). It shows the coupling between the polarization modes $\mathrm{LP}_{01\mathrm{x}}$ and $\mathrm{LP}_{01\mathrm{y}}$. Region B is formed by the 4×4 array on the bottom right corner and enclosed by the impulse-response matrix elements (h_{33}, h_{36}, h_{63}, h_{66}). Region B shows the coupling between the spatial and polarization modes $\mathrm{LP}_{11\mathrm{ax}}$, $\mathrm{LP}_{11\mathrm{ay}}$, $\mathrm{LP}_{11\mathrm{bx}}$, and $\mathrm{LP}_{11\mathrm{by}}$. The two remaining off-diagonal regions C and D, enclosed by (h_{13}, h_{16}, h_{23}, h_{26}) and (h_{31}, h_{32}, h_{61}, h_{62}), respectively, describe the crosstalk between LP_{01} and LP_{11} modes. In Fig. 9, we observe sharp and strong coupling peaks within regions A and B, and typically 100 to 1000 times weaker, 2.6 ns wide distributed coupling in regions C and D. The width of the distributed coupling shown in regions C and D corresponds to the DGD for 96 km of six-mode FMF as measured in Section II and represents coupling occurring at various locations along the fiber. If the light travels mostly in the LP_{01} mode, it arrives earlier, whereas it arrives delayed by the DGD if it travels mostly in the slower LP_{11} mode. Also regions A and B show weaker distributed coupling next to the strong coupling peaks. We believe this weaker distributed coupling is caused by light that couples back and forth between LP_{01} and LP_{11} or LP_{11} and LP_{01} modes, respectively. For LP_{01} modes (region A), the distributed coupling whose width is also consistent with the DGD of 96-km six-mode FMF is located on the right of the main pulse, whereas it is located on the left of the main pulse for the LP_{11} modes (region B). Finally, Fig. 9 also confirms the excellent alignment of the mode coupler. Any misalignment in the coupler would create a narrow and higher crosstalk peak either at the beginning or at the end of the distributed coupling in regions C and D. The channel estimation gives a very clear picture of the crosstalk introduced by the MMUX and the propagation through the six-mode FMF and allows a better understanding of the observed performance of the MIMO DSP presented in Section VI.

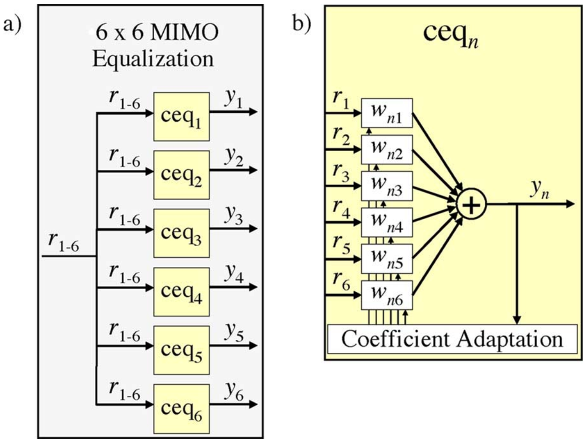

Fig. 10. Architecture of the MIMO equalization block.

VI. DSP AND BER MEASUREMENTS

The 6×6 MIMO DSP architecture is an extension of the 2×2 implementation frequently found in coherent PDM receivers and is shown in Fig. 10. The six received signals r_{1-6} from the three PD-CRXs are fed into six column equalizers (ceq_{1-6}) [see Fig. 10(a)]. Each column equalizer produces one output signal y_{1-6}. The structure of the column equalizer ceq_n is shown in Fig. 10(b) and consists of six feed-forward equalizers (FFEs). Each FFE has L taps described by the complex coefficient vectors w_{n1-n6} with length L. The sum of the outputs of the six FFEs produces the recovered signal y_n. In total, 36 FFEs are required and the equalizer coefficients w_{n1-n6} are adapted by running the data-aided LMS algorithm [28] over the first 500 000 symbols and then switching to decision-directed LMS for the remaining symbols. This guarantees a rapid initial convergence of the equalizer coefficients w_{n1-n6}. For a practical transmission system, this would be realized, for example, by a predefined training pattern during the startup phase. Also, the standard LMS algorithm was modified to include carrier phase estimation based on the fourth power algorithm [29]. A more detailed description of the complete algorithm can be found in [21]. Finally, the BER is evaluated over the last one million symbols of the data acquisition.

Fig. 11 shows the experimental BER curves after offline 6×6 MIMO processing with $L = 120$, where we made use of the noise loading section described in Section IV to change the optical signal-to-noise ratio (OSNR). All six received data streams are recovered from the three PD-CRXs. The BER curves are plotted as a function of $\mathrm{OSNR}_{\mathrm{pol}}$, which is defined as the OSNR (0.1 nm optical noise reference bandwidth), except that only the noise that is copolarized with the corresponding signal component is included. Fig. 11 also includes the B2B measurements and the theoretical limit for coherent detection of QPSK as a reference. All B2B measurements show less than 0.8 dB penalty at a BER of 10^{-3}, and all six BER curves after transmission are within 1.2 dB from the B2B measurements. This excellent performance shows that crosstalk present in the six-mode FMF can

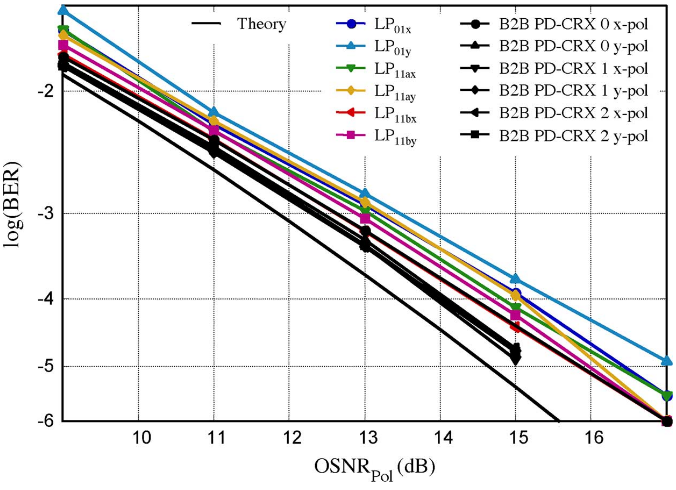

Fig. 11. BER curves for six-channel PDM–SDM transmission of 20 Gbaud QPSK over 96 km of six-mode FMF. Also shown for reference are the B2B measurements and the theoretical limit.

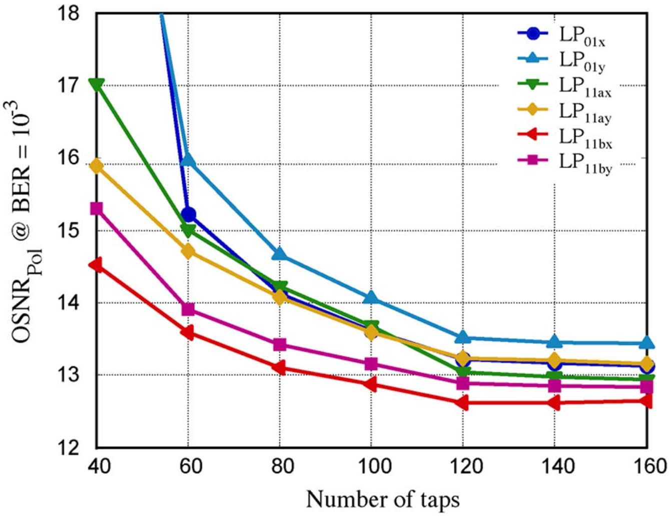

Fig. 12. Required $\mathrm{OSNR}_{\mathrm{pol}}$ for 96 km of six-mode FMF at a BER of 10^{-3} as a function of the number of equalizer taps L.

be successfully compensated with very low impact on system performance.

In order to investigate the impact of the number of half-symbol-spaced taps L, we evaluate the required $\mathrm{OSNR}_{\mathrm{pol}}$ for a BER of 10^{-3} as a function of L. The results are reported in Fig. 12. It can be seen that no significant performance improvement can be obtained for more than $L = 120$ equalizer taps. A length of $L = 120$ taps corresponds to 3 ns in time, which is close to the width of the crosstalk peaks of 2.6 ns as presented in the impulse-response matrix estimation results in Section V. The discrepancy can be explained if chromatic dispersion, which is electronically compensated for the impulse-response matrix estimation, but not for the MIMO DSP, is taken into account. Furthermore, a length $L = 120$ taps is also consistent with the DGD measured independently in Section II.

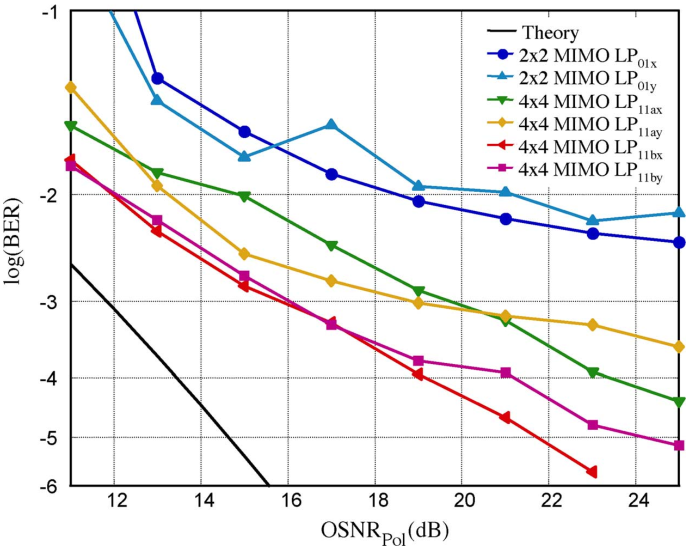

Fig. 13. BER curves for 96 km of six-mode FMF obtained by applying 2×2 MIMO DSP for the LP_{01} mode and 4×4 MIMO DSP for the LP_{11} mode.

Next, we investigate if the coupling between the LP_{01} and the LP_{11} modes is small enough to allow a reduction in DSP complexity by using only 2×2 MIMO on the LP_{01} mode and an independent 4×4 MIMO DSP on the LP_{11} mode, as presented in [8]. Fig. 13 shows the BER when 2×2 and 4×4 MIMO DSP is used. The performance is dramatically degraded. A large penalty of 8 dB at a BER of 10^{-3} is observed for the LP_{11} mode, whereas a BER of 10^{-3} cannot be reached for the LP_{01} mode. Also we observe a large variability of the BER for different values of $\mathrm{OSNR}_{\mathrm{pol}}$, which we attribute to the fact that for each $\mathrm{OSNR}_{\mathrm{pol}}$ setting, measurements are taken several minutes apart from each other. Therefore, the crosstalk conditions, which are continuously changing in the fiber on a millisecond time scale, may have been different, leading to a variation in BER. Also, we would like to mention that this result is only valid for the low-DGD six-mode FMF used in this experiment. For FMF with larger modal propagation constant difference $\Delta\beta$, a weaker coupling between the LP_{01} and the LP_{11} modes is predicted, and good performance can be expected.

VII. CONCLUSION

We have demonstrated single-wavelength six-channel spatial- and polarization-mode-multiplexed transmission of 6×40-Gb/s QPSK signals over 96 km FMF with less than 1.2 dB penalty. The impulse-response matrix of the low-DGD FMF was determined, revealing in detail the coupling between the six guided spatial and polarization modes. The results were achieved using offline coherent MIMO DSP and high-performance mode couplers based on phase plates.

ACKNOWLEDGMENT

The authors would like to thank G. Raybon, C. Xie, S. Chandrasekhar, X. Liu, and R. Tkach for support with the experiment.

REFERENCES

[1] R.-J. Essiambre, G. Kramer, P. J. Winzer, G. J. Foschini, and B. Goebel, “Capacity limits of optical fiber networks,” *J. Lightw. Technol.*, vol. 28, no. 4, pp. 662–701, Feb. 2010.

[2] R. Tkach, “Scaling optical communications for the next decade and beyond,” *Bell Labs Tech. J.*, vol. 14, no. 4, pp. 3–9, 2010.

[3] A. Chraplyvy, “The coming capacity crunch,” presented at the presented at the 35th Eur. Conf. Opt. Commun., Vienna, Austria, 2009.

[4] P. J. Winzer, “Energy-efficient optical transport capacity scaling through spatial multiplexing,” *IEEE Photon. Technol. Lett.*, vol. 23, no. 13, pp. 851–853, Jul. 2011.

[5] M. de Boer, C. P. Tsekrekos, A. Martinez, H. Kurniawan, J. W. M. Bergmans, A. M. J. Koonen, H. P. A. van den Boom, and F. M. J. Willems, “A first demonstrator for a mode group diversity multiplexing communication system,” presented at the IEE Seminar Optical Fibre Commun. Electron. Signal Process., London, U.K., 2005.

[6] S. Schöllmann, S. Soneff, and W. Rosenkranz, “10.7 Gb/s over 300 m GI-MMF using a 2 × 2 MIMO system based on mode group diversity multiplexing,” in *Proc. Opt. Fiber Commun./Nat. Fiber Opt. Eng. Conf.*, 2007, pp. 1–2.

[7] A. Li, A. Al Amin, X. Chen, and W. Shieh, “Reception of mode and polarization multiplexed 107 Gb/s CO-OFDM signal over a two-mode fiber,” in *Proc. Opt. Fiber Commun. Conf. Expo./Nat. Fiber Opt. Eng. Conf.*, 2011, pp. 1–3.

[8] M. Salsi, C. Koebele, D. Sperti, P. Tran, P. Brindel, H. Mardoyan, S. Bigo, A. Boutin, F. Verluise, P. Sillard, M. Bigot-Astruc, L. Provost, F. Cerou, and G. Charlet, “Transmission at 2 × 100 Gb/s, over two modes of 40 km-long prototype few-mode fiber, using LCOS based mode multiplexer and demultiplexer,” presented at the Proc. Opt. Fiber Commun. Conf./Nat. Fiber Opt. Eng. Conf., Los Angeles, CA, 2011.

[9] N. Hanzawa, K. Saitoh, T. Sakamoto, T. Matsui, S. Tomita, and M. Koshiba, “Demonstration of mode-division multiplexing transmission over 10 km two-mode fiber with mode coupler,” in *Proc. Opt. Fiber Commun. Conf. Expo./Nat. Fiber Opt. Eng. Conf.*, 2011, pp. 1–3.

[10] B. Zhu, T. F. Taunay, M. Fishteyn, X. Liu, S. Chandrasekhar, M. F. Yan, J. M. Fini, E. M. Monberg, F. V. Dimarcello, K. Abedin, and P. W. Wisk, “Space-, wavelength-, polarization-division multiplexed transmission of 56 Tb/s over a 76.8 km seven-core fiber,” in *Proc. Opt. Fiber Commun. Conf. Expo./Nat. Fiber Opt. Eng. Conf.*, 2011, pp. 1–3.

[11] J. Sakaguchi, Y. Awaji, N. Wada, A. Kanno, T. Kawanishi, T. Hayashi, T. Taru, T. Kobayashi, and M. Watanabe, “109 Tb/s (7 × 97 × 172 Gb/s SDM/WDM/PDM) QPSK transmission through 16.8 km homogeneous multi-core fiber,” in *Proc. Opt. Fiber Commun. Conf. Expo./Nat. Fiber Opt. Eng. Conf.*, 2011, pp. 1–3.

[12] A. R. Shah, R. C. J. Hsu, A. Tarighat, A. H. Sayed, and B. Jalali, “Coherent optical MIMO (COMIMO),” *J. Lightw. Technol.*, vol. 23, no. 8, pp. 2410–2419, Aug. 2005.

[13] P. J. Winzer and G. J. Foschini, “MIMO capacities and outage probabilities in spatially multiplexed optical transport systems,” *Opt. Exp.*, vol. 19, no. 17, pp. 16680–16696, 2011.

[14] B. Franz, D. Suikat, R. Dischler, F. Buchali, and H. Buelow, “High speed OFDM data transmission over 5 km GI-multimode fiber using spatial multiplexing with 2 × 4 MIMO processing,” in *Proc. 36th Eur. Conf. Opt. Commun.*, 2010, pp. 1–3.

[15] G. Keiser, *Optical Fiber Communications*, 3rd ed. New York: McGraw Hill, 2000.

[16] D. Marcuse, *Theory of Dielectric Optical Waveguides*, P. F. Liao and P. L. Kelley, Eds. New York: Academic, 1991.

[17] W. Q. Thornburg, C. B. J. , and X. D. Zhu, “Selective launching of higher-order modes into an optical fiber with an optical phase shifter,” *Opt. Lett.*, vol. 19, no. 7, pp. 454–456, 1994.

[18] W. Mohammed, M. Pitchumani, A. Mehta, and E. G. Johnson, “Selective excitation of the LP_{11} mode in step index fiber using a phase mask,” *Opt. Eng.*, vol. 45, no. 7, pp. 074602-1–074602-7, 2006.

[19] Y. Awaji, N. Wada, and Y. Toda, “Demonstration of spatial mode division multiplexing using Laguerre–Gaussian mode beam in telecom-wavelength,” in *Proc. IEEE 23rd Annu. Meet. Photon. Soc.*, 2010, pp. 551–552.

[20] J. Salz, “Digital transmission over cross-coupled linear channels,” *AT&T Tech. J.*, vol. 64, pp. 1147–1159, 1985.

[21] S. Randel, R. Ryf, A. Sierra, P. J. Winzer, A. H. Gnauck, C. A. Bolle, R.-J. Essiambre, D. W. Peckham, A. McCurdy, and R. Lingle, “6 × 56-Gb/s mode-division multiplexed transmission over 33-km few-mode fiber enabled by 6 × 6 MIMO equalization,” *Opt. Exp.*, vol. 19, no. 17, pp. 16697–16707, 2011.

[22] R. Ryf, S. Randel, A. H. Gnauck, C. Bolle, R.-J. Essiambre, P. J. Winzer, D. W. Peckham, A. McCurdy, and R. Lingle, “Space-division multiplexing over 10 km of three-mode fiber using coherent 6 × 6 MIMO processing,” in *Proc. Opt. Fiber Commun. Conf./Nat. Fiber Opt. Eng. Conf.*, 2011, pp. 1–3.

[23] S. Ramachandran, J. W. Nicholson, S. Ghalmi, and M. F. Yan, “Measurement of multipath interference in the coherent crosstalk regime,” *IEEE Photon. Technol. Lett.*, vol. 15, no. 8, pp. 1171–1173, Aug. 2003.

[24] R. Olshansky, “Mode coupling effects in graded-index optical fibers,” *Appl. Opt.*, vol. 14, no. 4, pp. 935–945, 1975.

[25] V. A. Soifer and M. A. Golub, *Laser Beam Mode Selection by Computer Generated Holograms*. Boca Raton, FL: CRC Press, 1994.

[26] J. A. Buck, *Fundamentals of Optical Fibers*. New York: Wiley, 1995.

[27] A. Sierra, S. Randel, P. J. Winzer, R. Ryf, A. H. Gnauck, and R.-J. Essiambre, “On the use of delay-decorrelated I/Q test sequences for QPSK and QAM signals,” *IEEE Photon. Technol. Lett.*, submitted for publication.

[28] N. Benvenuto and G. Cherubini, *Algorithms for Communications Systems and Their Applications*. New York: Wiley, 2002.

[29] A. J. Viterbi and A. M. Viterbi, “Nonlinear estimation of PSK-modulated carrier phase with application to burst digital transmission,” *IEEE Trans. Inf. Theory*, vol. 29, no. 4, pp. 543–551, Jul. 1983.

Roland Ryf (M’03) received the diploma and the Ph.D. degree in physics from the Swiss Federal Institute of Technology, Zürich, Switzerland, where he was involved in photorefractive self-focusing and spatial solitons, parallel optical processing based on holographic storage, and fast optical correlation.

Since May 2000, he has been a member of the Photonic Subsystems and the Advanced Photonics Research Department, Bell Laboratories, Alcatel-Lucent, Holmdel, NJ, where he is involved in the optical design and prototyping of optical microelectromechanical systems (MEMs) and liquid crystal on silicon-based devices. In particular, he has been involved in large port count cross-connect switches, programmable high-resolution spectral filters, wavelength selective switches, MEMS-based infrared sensors, and laser projection displays. He has been most recently involved in the free-space couplers and optical transmission in multicore and multimode fibers. He has more than 60 publications and more than 15 patents in the field of optical communication.

Sebastian Randel (SM’11) received the Ph.D. degree (with highest honors) in electrical engineering from Technische Universität Berlin, Berlin, Germany, in 2005, for his study on nonlinear optical time division multiplexing transmission.

He is a Member of the Technical Staff at Bell Laboratories, Alcatel-Lucent, Holmdel, NJ. He is currently involved in the research on ultrahigh capacity optical transmission systems. From 2005 to 2010, he was a Research Scientist at Siemens AG, Munich, Germany, where he was involved in physical layer aspects of optical access, in-house, automotive, and industrial networks.

Dr. Randel was a Founding Chairman of the DKE Working Group Polymer Optical Fiber and is a member of the Association for Electrical, Electronic and Information Technologies/Information Technology Society.

Alan H. Gnauck (F’09) joined Bell Laboratories, Alcatel-Lucent, Holmdel, NJ, in 1982, where he is currently a Distinguished Member of the Technical Staff in the Transmission Systems Research Group. He has performed record-breaking optical transmission experiments at single-channel rates of from 2 to 400 Gb/s. He has investigated coherent detection, chromatic-dispersion compensation techniques, cable television hybrid fiber-coax architectures, wavelength division multiplexing (WDM) systems, and system impacts of fiber nonlinearities. His WDM transmission experiments include the first demonstration of terabit transmission in 1996. More recently, he has demonstrated 25-Tb/s transmission in 2007. He is currently involved in the study of WDM systems with single-channel rates of 100 Gb/s and higher, using advanced modulation formats and coherent detection. He has authored or coauthored more than 200 journal and conference papers, and holds 25 patents in optical communications.

Mr. Gnauck is a Fellow of the Optical Society of America (OSA) and served as an associate editor for the IEEE PHOTONICS TECHNOLOGY LETTERS (2000–2009). He was a technical subcommittee member for the Optical Fiber Communications Conference in 2000, 2001, and 2003, and served as subcommittee Chair in 2004. He received the OSA Engineering Excellence Award in 2003.

Cristian Bolle was born in Buenos Aires, Argentina, in 1966. He received the M.S. and Ph.D. degrees in physics from the Instituto Balseiro, Bariloche, Argentina, in 1990 and 1995, respectively.

Between 1995 and 1997 he was a Postdoctoral Researcher in the Charles Lieber Group, Harvard University. In 1997, he joined the Physical Sciences Group, Bell Laboratories, Lucent Technologies, Homdel, NJ. He was involved in the research of mesoscopic superconductors at low temperatures with high-

Q micromechanical oscillators and later on in the development of the micromachine-based Lambda router all optical switch. He has also been involved in thermal management and cost reduction activities closely related to Lucent products. He is currently part of the Microsystems and Nanotechnology Research Lab, Bell Laboratories, Alcatel-Lucent, Murray Hill, NJ, where he is involved in a variety of projects related to micromachines and telecommunications. In this area, he has more than a dozen U.S. patents.

Alberto Sierra (S'11) received the B.S. and M.E. equivalent engineering degrees in telecommunications and computer science from the Universitat Politècnica de Catalunya, Barcelona, Spain, in 2011. His engineer thesis was on space division multiplexing for coherent optical communication.

During his studies, he was at the Institute of Robotics and Industrial computing, where he was involved in parallel manipulators, and at the Institute of Photonic Sciences, where his research was focused on microwave subwavelength transmission. In 2011, he was doing an internship for nine months at Alcatel-Lucent Bell Laboratories, Holmdel, NJ, where he was involved in spatial multiplexing and offset quadrature amplitude modulation.

Sami Mumtaz received the B.Sc. degree in electrical engineering and Ph.D. degree from Telecom ParisTech, Paris, France, in 2007 and 2011, respectively. His Ph.D. dissertation focused on coding techniques for optical transmission systems.

He is currently a Postdoctoral Researcher in the group of Prof. Agrawal at The Institute of Optics, University of Rochester, Rochester, NY, doing research in collaboration with R.-J. Essiambre from Bell Laboratories, Alcatel-Lucent, Holmdel, NJ. His research interests include coding techniques, such as forward error correction and space-time coding, and equalization techniques applied to coherent optical transmission systems. He is also doing research on understanding nonlinear propagation in various optical fibers.

Mina Esmaeelpour received the B.S. degree in physics and M.S. degree in solid-state physics from Tabriz University, Tabriz, Iran, in 2007 and 2009, respectively. She is currently working toward the Ph.D. degree at the Department of Physics, Lehigh University, Bethlehem, PA.

She is a member of the Nonlinear Optics and Photonics Group, doing research under the supervision of Prof. J. Toulouse.

Ellsworth C. Burrows received the A.A.S. degree in electronics technology from Technical Career Institutes, New York, NY, in 1985.

In November 1985, he joined AT&T Bell Laboratories, where his research was focused on semiconductor processing and optoelectronic integrated circuits for lightwave systems. He is currently in the Transmission System Research Department, Bell Laboratories, Alcatel-Lucent Technologies, Holmdel, NJ.

René-Jean Essiambre (S'95–SM'06) received the B.S. and Ph.D. degrees in physics and optics from Université Laval, Québec City, QC, Canada.

During his Ph.D. studies, he spent one year at McGill University, Montréal, QC, Canada, where he was involved in research on solid-state physics. From 1995 to 1997, he was a Postdoctoral Fellow with Prof. Agrawal at The Institute of Optics, University of Rochester, Rochester, NY. Since 1997, he has been at Bell Laboratories, Alcatel-Lucent, Holmdel, NJ. His earlier research was focused on optical switching, soliton communication systems, high-power fiber lasers, and mode-locked fiber lasers. He is the author or coauthor of more than 100 scientific publications and several book chapters. He is a Distinguished Member of Technical Staff at Bell Laboratories. His current research interests include high-speed transmission (100 Gb/s and above) and physical layer design of fiber-optic communication systems, including Raman amplification, Rayleigh backscattering, fiber nonlinearities, network design, advanced modulation formats, information theory, and coding.

Dr. Essiambre has served on many conference committees including European Conference on Optical Communication, Optical Fiber Communication, Conference on Lasers and Electro-Optics, and IEEE Lasers and Electro-Optics Society. He is the Program Co-Chair of CLEO: Science and Innovations 2012. He is a Fellow of the Optical Society of America (OSA). He is the recipient of the 2005 OSA Engineering Excellence Award.

Peter J. Winzer (F'09) received the Ph.D. degree in electrical engineering from the Vienna University of Technology, Vienna, Austria, in 1998.

Supported by the European Space Agency, he investigated space-borne Doppler lidar and laser communications using high-sensitivity digital modulation and detection. In 2000, he joined Bell Laboratories, Alcatel-Lucent, Holmdel, NJ, where his research focused on many aspects of fiber-optic networks, including Raman amplification, optical modulation formats, advanced optical receiver concepts, digital signal processing and coding, as well as on robust network architectures for dynamic data services. He demonstrated several high-speed and high-capacity optical transmission records from 10 to 100 Gb/s and beyond, including the first 100G and the first 400G electronically multiplexed optical transmission systems and the first field trial of live 100G video traffic over an existing carrier network. In 2007, he became the Distinguished Member of Technical Staff, Bell Laboratories and since 2010 he has been the Head of the Optical Transmission Systems and Networks Research Department.

Dr. Winzer is a Member of the Optical Society of America. He has widely published and patented and is actively involved in technical and organizational tasks with the IEEE Photonics Society and the OSA.

David W. Peckham (SM'04) received the B.S. and M.E. degrees in electrical engineering from the University of Florida, Gainesville.

In 1982, he joined the Bell Labs Transmission Media Laboratory, where he was involved in optical fiber measurement techniques. Since 1989, his research has been focused on the design, process development, and commercialization of optical fibers for high-capacity transmission systems. He is currently a Consulting Member of Technical Staff/Research Fellow in the Optical Fiber Design Group, OFS, Norcross, GA.

Dr. Peckham received the 2002 Optical Society of America Engineering Excellence Award recognizing his contributions in the design and commercialization of fibers enabling high-speed, wideband wavelength division multiplexing networks.

Alan H. McCurdy (M'91) received the Graduate's degree in chemical engineering and physics from Carnegie-Mellon University, Pittsburgh, PA, and the Ph.D. degree in applied physics from Yale University, New Haven, CT, in 1987, studying plasma physics.

He spent nine years in the faculty of the Department of Electrical Engineering, University of Southern California, with a one-year sabbatical at the Naval Research Laboratory, Washington, DC. Since 1998, he has been involved in the research on telecommunications first at Lucent Technologies, then Avaya, Inc., and most recently at OFS, Norcross, GA, where he is currently a Distinguished Member of Technical Staff in the Optical Fiber Design Group. His academic study involved characterization and control of high-power, electron-beam driven microwave oscillators and amplifiers. He was also involved in transmission problems in copper-based enterprise network systems, and statistical and nonlinear problems in optical communications.

Dr. McCurdy has received a variety of teaching and research awards throughout his career.

Robert Lingle, Jr., (M'02) received the Ph.D. degree in physics from Louisiana State University, Baton Rouge.

He is the Director of Fiber Design and Systems Research, OFS, Norcross, GA, as well as an Adjunct Professor of Electrical and Computer Engineering at the Georgia Institute of Technology, Atlanta. He has a research background in short pulse lasers and their application to fundamental processes in liquids and interfaces. He was a Postdoctoral Researcher in surface physics at University of California, Berkeley. At Bell Labs and currently OFS, he was involved in sol–gel materials chemistry and managed the development and commercialization of new optical fibers for fiber-to-the-home, long haul, and submarine networks. His current research interests include ultra large area fibers, few-mode fibers, and the confluence of optical and electrical methods for mitigating impairments in transport.